DESIGN OF THE ACTIVE ELEVON ROTOR FOR LOW VIBRATION

Mark V. Fulton
Research Scientist

Army/NASA Rotorcraft Division
Aeroflightdynamics Directorate (AMRDEC)
US Army Aviation and Missile Command
Ames Research Center, Moffett Field, California

Introduction

Helicopter fuselages vibrate more than desired, and traditional solutions have limited effectiveness and can impose an appreciable weight penalty. Alternative methods of combating high vibration, including Higher Harmonic Control (HHC) via harmonic swashplate motion and Individual Blade Control (IBC) via active pitch links, have been studied for several decades. HHC via an on-blade control surface was tested in 1977 on a full scale rotor using a secondary active swashplate and a mechanical control system (Ref. 1).

Recent smart material advances have prompted new research into the use of on-blade control concepts. Recent analytical studies (Refs. 2-3) have indicated that the use of on-blade control surfaces produces vibration reduction comparable to swashplate-based HHC but for less power. Furthermore, smart materials (such as piezoceramics) have been shown to provide sufficient control authority for preliminary rotor experiments. These experiments were initially performed at small scale for reduced tip speeds (Refs. 4-8). More recent experiments have been conducted at or near full tip speeds (Refs. 9-10), and a full-scale active rotor is under development by Boeing (Ref. 11) with Eurocopter et al. (Ref. 12) pursuing a similarly advanced full-scale implementation.

The US Army Aeroflightdynamics Directorate has undertaken a new research program called the Active Elevon Rotor (AER) Focus Demo. This program includes the design, fabrication, and wind tunnel testing of a four-bladed, 12.96 ft diameter rotor with one or two on-blade elevons per blade. The rotor, which will be Mach scaled, will use 2-5/rev elevon motion for closed-loop control and will be tested in late 2001. The primary goal of the AER Focus Demo is the reduction of vibratory hub loads by 80% and the reduction of vibratory blade structural loads. A secondary goal is the reduction of rotor power. The third priority is the measurement and possible reduction of Blade Vortex Interaction (BVI) noise.

The present study is focused on elevon effectiveness, that is, the elevon's ability to reduce all six components of the nonrotating 4/rev hub loads. Some design parameters have been kept fixed in this study, while others have been varied to determine their influence on elevon effectiveness. The fixed parameters include all blade structural properties except for torsion stiffness; the varied parameters include torsion stiffness, elevon aerodynamic location, and the number and individual authority of elevon aerodynamic surfaces. This paper describes the preliminary design process being used for the AER, and describes and quantifies the emerging active rotor characteristics.

Rotor Description

The Active Elevon Rotor (AER) will be a four-bladed articulated rotor with a 12.96 ft diameter, a rectangular planform, and linear twist. One airfoil (the VR-18 with a 0.04 *c* tab at -3 deg, Ref. 13) will be used for the entire blade aerodynamic cross section. Blade properties will be uniform (except for inherent differences at the blade root and,

Presented at the AHS Aeromechanics Specialists' Meeting, November 13-15, 2000, Atlanta, Georgia.

possibly, in the active section). Structural properties for the baseline AER will be those used for the 27% Apache rotor (Ref. 14). The nominal rotor speed will be 1,070 RPM (17.83 Hz). Rotor properties are given in Table 1. The rotor radius, chord, and tip speed match the ideally scaled 27% Apache (Ref. 14) and are compatible with the Army Rotorcraft Test Stand (ARTS) to be used for the AER.

Blade structural properties are varied from a baseline during preliminary design. The baseline blade properties are taken from the ideally scaled 27% Apache properties (Ref. 14) and are listed in Table 2 for the uniform section. Structural variations from the baseline will be discussed later.

Elevon Sizing and Aerodynamics

The elevon is a plain trailing-edge control surface, which indicates that there is no aerodynamic balance; specifically, the elevon is assumed to pivot about the airfoil mid thickness and to have a semi-circular shape forward of the hinge point. Two-dimensional (2-D) thin-airfoil theory indicates that elevons are more efficient for smaller elevon chords. That is, more lift and moment are produced for a given amount of elevon work for smaller elevons. It was believed that an elevon size of 0.15 c or 0.20 c would be optimum for the present investigation. Since thin-airfoil theory is not sufficiently accurate for calculating elevon aerodynamic coefficients, a 2-D CFD (Computational Fluid Dynamics) study was performed by Ray Wong and C.P. van Dam (UC Davis) using MSES (a viscous/inviscid interaction, integral boundary layer code, Ref. 15). Preliminary results from their study indicated that the 0.15 c elevon would be significantly more efficient (than a 0.20 c elevon) for representative combinations of angle of attack and Mach number (Ref. 16). Because of these preliminary CFD results and since a 0.15 c actuator configuration was under investigation by Domzalski Machine as described in the next section, the 0.15 c elevon was selected for the present preliminary rotor blade design study. Elevon aerodynamic coefficients used in the study were $c_{l\delta}$ = 2.29/rad and $c_{m\delta}$ = -0.427/rad (Ref. 16).

Actuation

The actuator used for the AER is part of the Domzalski CAT (Conformal Actuator Technology) series (Ref. 17). This actuator uses a piezoceramic material and has been sized to provide ±5 deg deflection of a 0.15 c elevon operating at 463 lb/ft^2, the dynamic pressure at 0.86 R in hover. The actuator is radially co-located with the elevon. Domzalski conceptual sizing for the AER provides a minimum elevon span of 3.1 in (or 0.04 R), with multiples of this minimum size available as required. This minimum span will be referred to as a "single-wide" actuator; a total of four such single-wide actuators have been anticipated, or a total span of 0.16 R, although the preliminary design will need to determine the adequacy of this estimate. The total actuator weight used for this study was fixed at 0.52 lb, which corresponds to a 12.4 in span, including balance weights for a chord-wise center of gravity at 0.263 c. This weight was assumed to be evenly distributed between .68 and .84 R. The actuator weight and general configuration may remain unchanged for various elevon positions, although appropriate modifications can be made to keep the actuator stiffness equal to the aerodynamic stiffness to maximize work output. Thus, as the elevon aerodynamic location was varied in this study, the maximum elevon angle was varied in proportion to $1/r_\delta$, where r_δ is the radial position of the elevon mid-span.

Modeling

All calculations were performed using CAMRAD II (Ref. 18) with a common structural definition. This model consisted of eleven (11) structural elements for the blade, and several elements defining the articulating portions of the hub, with the non-articulating portion of the hub and the control system assumed rigid.

The aerodynamic surface of the blade was modeled as a lifting line with twenty (20) aerodynamic panels. The blade aerodynamic loads were calculated using table look-up to account for static nonlinearities due to angle of attack and Mach number; dynamic stall was neglected. The airfoil table was developed by Boeing for a variant of the VR-12 similar to the version being used for the AER, with CAMRAD II adjustment for zero-lift angle and a moment coefficient increment to account for a tab angle

change. Unsteady aerodynamics was represented by the thin airfoil model.

Wake modeling varied with the analysis being performed. For all hover calculations, uniform inflow was used. For forward flight calculations, a free wake model was used.

Elevon aerodynamics was modeled using the linear coefficients given in a previous section.

Trim was calculated for the nonlinear structural elements in hover (without modal analysis), but 8 trim blade modes were used when calculating harmonic balance in forward flight. Forward flight trim targets were $C_T/\sigma = 0.10$ (T = 1,534 lb), a propulsive force of 2.0 ft^2 times the dynamic pressure, and zero 1/rev flapping; trim controls were collective, longitudinal shaft tilt (positive aft), and cyclic pitch angles. The fuselage equivalent flat plate area of 2.0 ft^2 is 0.015 times the rotor area and yields -4.0 deg shaft tilt for the baseline model at an advance ratio of 0.30. Hover trim was calculated for a fixed collective pitch of 9.5 deg, zero shaft tilt, and zero cyclic pitch angles, yielding $C_T/\sigma = 0.10$ for the baseline model using uniform inflow.

Frequency response functions were only calculated in hover and were based on a flutter solution which approximates the control (i.e. the elevon) as a quasi-static variable, although the other degrees of freedom are treated as dynamic variables. Calculations were made for 4/rev hub load response to 4/rev elevon modes, all in the nonrotating frame. Both 4/rev thrust (T) and 4/rev torque (Q) loads are affected by the 4/rev elevon collective mode (δ_o), and the in-plane hub loads (shears and moments) are affected by the 4/rev elevon cyclic modes (δ_{1s} and δ_{1c}). The symmetry of hover means that the response of the lateral force to longitudinal elevon cyclic (Y/δ_{1c}) is equal to the response of the longitudinal force to lateral elevon cyclic ($-H/\delta_{1s}$); similarly, $Y/\delta_{1s} = H/\delta_{1c}$. Analogous relations exist between the roll moment (M_x) and pitch moment (M_y). Thus, the nonrotating hover transfer functions are governed by six unique relations, T/δ_o , Q/δ_o , H/δ_{1c} , H/δ_{1s} , M_x/δ_{1c} , and M_x/δ_{1s} , for each elevon radial location. Of the two longitudinal responses, H/δ_{1c} and H/δ_{1s} , one will generally be larger than the other, suggesting a preferred control (either δ_{1s} or δ_{1c}) when circumstances permit; likewise for M_x/δ_{1c} and M_x/δ_{1s} . The elevon cyclic mode which maximizes a given in-plane response will be denoted as δ_{1x}. This simplification will be used during some of the following analysis when it appears advantageous and reasonable.

Natural Frequencies

The natural frequencies of the baseline structural model are shown in Figure 1 as solid lines, with alternative solutions shown for the 1st torsion natural frequency at the nominal rotor speed; all frequencies were calculated in hover, at 9.5 deg collective pitch, in a vacuum. The alternative torsion frequencies were achieved by means of changes of the torsion stiffness of the blade; the 1st torsion natural frequency is shown to vary between 2.5 and 5.5/rev in roughly 0.2/rev increments.

Steady-State Vibratory Hub Loads

The steady-state, 4/rev hub loads were calculated for the baseline model and are presented in Figure 2 and Figure 3 for advance ratios between 0.125 and 0.32. The two vertical lines indicate two advance ratios which will be further considered during the remainder of the paper – transition at $\mu = .125$ and cruise at $\mu = .25$. Transition is simply the lowest advance ratio calculated, and it yields the maximum 4/rev hub loads, both for the shears (Figure 2) and for the moments (Figure 3). Cruise is defined as the advance ratio for maximum range of the baseline configuration. Since the 4/rev vibratory hub loads have not increased significantly by $\mu = .32$, further calculations will be required before high speed flight can be considered during the design; the use of a dynamic stall model and a higher propulsive force will be considered for future calculations.

Elevon Effectiveness

Elevon effectiveness was calculated in hover for the six unique transfer functions previously described, T/δ_o , Q/δ_o , H/δ_{1c} , H/δ_{1s} , M_x/δ_{1c} , and M_x/δ_{1s} . Of these six unique relations, the most significant four were retained, T/δ_o , Q/δ_o , H/δ_{1x} , and M_x/δ_{1x} . Plots of two of these functions, H/δ_{1x} and T/δ_o , are given in Figure 4 and Figure 5 as a function of torsion natural frequency for various radial locations of a single-wide elevon. The transfer functions represented by these two figures have been normalized by their corresponding 4/rev hub load for the baseline model in transition ($\mu = .125$); H/δ_{1x} was normalized by the 4/rev longitudinal force to

create Figure 4, and T/δ_o was normalized by the 4/rev thrust to create Figure 5.

These two normalized transfer functions are given because they are representative and in conflict. They are representative because M_x/δ_{1x} follows somewhat similar trends to H/δ_{1x} , and Q/δ_o is very similar to T/δ_o . The two functions are in conflict in that the H/δ_{1x} effectiveness (Figure 4) peaks at torsion frequencies lower than those found for the T/δ_o effectiveness (Figure 5). In addition, H/δ_{1x} and T/δ_o differ in the range of peaks displayed for elevon locations between 0.62 and 0.94 R – T/δ_o has a range of peaks double that of H/δ_{1x} . Finally, note that two torsion frequencies have been labeled. The "baseline" vertical line simply marks the torsion frequency of the baseline model, or 4.79/rev; the "alternate" vertical line indicates a tentative design choice (of $\omega_{\phi 1}$ = 3.3/rev) based largely on Figure 4. This alternate design appreciably improves the H/δ_{1x} effectiveness (relative to the baseline) for all elevon locations. Although the alternate generally lowers the T/δ_o effectiveness, a later section will demonstrate that this is a reasonable compromise since normalized elevon effectiveness is higher for T/δ_o and Q/δ_o than for the remaining hub responses.

Importance of Elevon Location

Another way to explore the design space is to select a few structural configurations and to then plot the elevon effectiveness ratios versus single-wide (.04 R) elevon radial position. Two sets of such plots have been created, one set for the baseline (Figure 6 and Figure 7), and the other for the alternate (Figure 8 and Figure 9). Each set includes two plots, with the first plot emphasizing thrust and yaw (or torque), and the second focussing on the in-plane loads (longitudinal and lateral forces, and pitch and roll moments).

In the figures to be discussed, six elevon radial locations have been selected, and each single-wide (.04 R) elevon has been assigned a unique primary hub load target. (In the next section, elevon secondary and tertiary hub load targets will be discussed.) The use of six elevon locations is a simplification which will likely be abandoned during future work – a design goal for the AER is that only one or two independently controlled elevons be used on each blade. Towards this goal, the positioning of single-wide elevons is addressed in this section, with control authority (of single-wide elevons) being addressed in the next section.

As an example, consider the baseline results of Figure 6 and Figure 7. Both figures include six vertical lines which mark the span-wise center of six different single-wide (.04 R) elevon locations. Each of these lines intersects one (and only one) transfer function (curve) in a special place denoted by a circle and number. The second figure (Figure 7) reveals four such intersections, while the first figure (Figure 6) indicates two special intersections. These markings reveal a simplistic, first-order approach – use six elevons to control six hub loads and assign each elevon as the primary control for one (and only one) hub load. The numerical order reveals the selection order; thus the circle labeled "1" in Figure 7 indicates that the elevon at 0.74 R was chosen first and that it was assigned the primary responsibility for controlling the hub lateral force. The sequence of selections progresses from 1 to 6 as the elevon effectiveness ratio increases. This is an attempt to treat all hub loads as equally important and, therefore, to give preferential treatment for those nondimensional hub loads which are more difficult to reduce. Figure 6 and Figure 7 reveal that there is a significant variation in elevon effectiveness for each hub load, and that thrust and yaw moment are more easily reduced than the in-plane loads.

Results for the alternate design are shown in Figure 8-Figure 9. Note that the alternate in-plane transfer functions (Figure 9) are significantly larger than the corresponding baseline transfer functions (Figure 7). Also note that the preferred elevon locations for the alternate are .04 R farther outboard than for the baseline design, and that the elevon primary control assignments have been redistributed to better match the alternate transfer function characteristics.

Elevon Sizing

The elevon locations selected in the previous section, and other selections made using similar techniques, were used to calculate the number and individual authority of the elevon aerodynamic surfaces required to achieve significant vibratory hub load reduction. Four sizing cases are presented in Table 3-Table 6, and a summary of all cases is presented in Table 7 and Table 8.

Table 3-Table 6 use the standard, single-wide elevon described previously; namely, the elevon

chord is c_δ = .15 c, and the magnitude of the maximum, local elevon deflection is $|\delta_r|$ = (.86 R/r_δ) 5 deg. Primary and secondary elevon motions are designated as δ_p and δ_s , respectively, with their sum constrained to be less than or equal to δ_r for the standard elevon. The elevon-induced hub loads are calculated from the transfer functions multiplied by the elevon deflection. (The hub load symbols are defined in Table 7 and Table 8.) Finally, the controlled hub load is calculated by invoking superposition; namely, the controlled hub load equals the uncontrolled hub load (Figure 2 and Figure 3) minus the sum of the elevon-induced hub loads.

Consider the most demanding case – transition vibratory hub load reduction using the baseline elevon effectiveness for a total of six elevon locations (using the locations and assignments previously shown in Figure 6 and Figure 7). Because the transition loads are so high relative to the elevon-to-hub transfer functions, the approach is very simple – start by letting each elevon work on its primary responsibility with 100% of the maximum elevon deflection available for its radial location. This case is detailed in Table 3. The first four elevons (r_δ = 0.62 to 0.74 R) use 100% of their available elevon deflection, yet their targets (Y, M_x, M_y, and H, respectively) are not significantly reduced (as can be seen in the last column). If the two most outboard of this six-elevon set (i.e. r_δ = 0.78 and 0.82 R) were allowed to contribute 100% towards their primary targets, then the Thrust (T) and Torque (Q) would be significantly reduced. Instead, the two outboard elevons have been assigned only about 1/4 of their deflection towards their primary duty, with the balance being assigned to secondary loads in an attempt to reduce all loads to a similar fraction of their uncontrolled values. (Secondary contributions are italicized, while tertiary contributions are italicized and underlined as in Table 4.)

Table 7 ($\omega_{\phi 1}$ = 4.79/rev) and Table 8 ($\omega_{\phi 1}$ = 3.3/rev) summarize all of the sizing cases studied to date. Table 7 ($\omega_{\phi 1}$ = 4.79/rev) repeats the controlled/uncontrolled ratios previously given in Table 3 for each of the six 4/rev hub loads at transition (μ = .125), resulting in an average controlled response of 0.77 times the uncontrolled value. Note that this limited effectiveness was achieved using six standard single-wide elevons working at their full capacity. For cruise (μ = .25), Table 7 indicates that these same six elevons reduced the average controlled response to 0.53 times the uncontrolled value, and that ten elevons are able to reduce this fraction to 0.27. The final column in Table 7 achieves a final fraction of 0.19 using "big" elevons equivalent (on a work basis) to 10.3 standard elevons concentrated in six locations, with the biggest elevon having 2-1/2 times the effectiveness of the standard 0.15 c elevon (moving ±5 deg at 0.86 R). The big elevons are able to be more effective since the elevons are allowed to work hardest where they are most effective; that is, the peaks evident in Figure 7 can be best exploited with highly concentrated aerodynamic effectiveness.

A comparison of Table 8 ($\omega_{\phi 1}$ = 3.3/rev) with Table 7 ($\omega_{\phi 1}$ = 4.79/rev) indicates a significantly enhanced effectiveness with the reduced torsion frequency. For the alternate design, a standard set of six elevons reduces the 4/rev hub loads to 0.59 times the uncontrolled value for transition; 3.7 elevons produces a fraction of 0.20 for cruise; and 4.8 elevons essentially nulls cruise 4/rev hub loads. Thus, significant improvements are predicted for the reduced torsion frequency of 3.3/rev.

Effect of Torsion on Uncontrolled Hub Loads

The total vibratory hub loads are affected by the elevon-to-hub-load transfer functions (previously described) and the uncontrolled vibratory hub loads. The promise of an altered torsion frequency must, therefore, be weighed against any potential increases in the uncontrolled vibratory loads. Figure 10-Figure 13 address this issue by showing the variation of the 4/rev hub loads with torsion natural frequency for transition and cruise. These plots reveal that the 4/rev hub loads are generally reduced for the alternate design.

Concluding Remarks

The preliminary design of the Active Elevon Rotor (AER) has begun and initial procedures and results were described in this paper. The primary conclusion to date is that enhanced elevon effectiveness is achieved at a reduced torsion natural frequency of 3.3/rev. While vibratory hub load alleviation is the primary goal, other considerations must eventually be taken into account, including blade structural loads and rotor power.

References

1. McCloud, J.L., III and Weisbrich, A.L., "Wind Tunnel Test Results of a Full-Scale Multicyclic Controllable Twist Rotor," American Helicopter Society 34th Annual Forum, Washington, DC, May 1978.

2. Millott, T.A. and Friedmann, P.P., "Vibration Reduction in Helicopter Rotors Using an Actively Controlled Partial Span Trailing Edge Flap Located on the Blade," NASA CR 4611, June 1994.

3. Milgram, J. and Chopra, I., "Helicopter Vibration Reduction with Trailing Edge Flaps," American Helicopter Society Northeast Region Aeromechanics Specialists' Meeting, Stratford, Connecticut, October 1995.

4. Samak, D.K. and Chopra, I., "A Feasibility Study to Build a Smart Rotor: Trailing Edge Flap Actuation," SPIE Smart Structures and Materials Conference, Albuquerque, New Mexico, February 1993.

5. Ben-Zeev, O. and Chopra, I., "Advances in the Development of an Intelligent Helicopter Rotor Employing Smart Trailing-Edge Flaps," Smart Materials & Structures, Vol. 5, (1), 1996.

6. Koratkar, N.A. and Chopra, I., "Analysis and Testing of a Froude Scaled Helicopter Rotor with Piezoelectric Bender Actuated Trailing Edge Flaps," Journal of Intelligent Material Systems and Structures, Vol. 8, (7), 1997.

7. Fulton, M.V. and Ormiston, R.A., "Hover Testing of a Small-Scale Rotor with On-Blade Elevons," American Helicopter Society 53rd Annual Forum, Virginia Beach, Virginia, April-May 1997.

8. Fulton, M.V. and Ormiston, R.A., "Small-Scale Rotor Experiments with On-Blade Elevons to Reduce Blade Vibratory Loads in Forward Flight," American Helicopter Society 54th Annual Forum, Washington, DC, May 1998.

9. Prechtl, E.F. and Hall, S.R., "Hover Testing of a Mach-Scaled Rotor with an Active Trailing Edge Flap," Eighth ARO Workshop on the Aeroelasticity of Rotorcraft Systems, State College, Pennsylvania, October 1999.

10. Koratkar, N.A. and Chopra, I., "Wind Tunnel Testing of a Mach-Scaled Rotor Model with Trailing-Edge Flaps," American Helicopter Society 56th Annual Forum, Virginia Beach, Virginia, May 2000.

11. Straub, F.K., "Development of a Full Scale Smart Rotor System," Eighth ARO Workshop on the Aeroelasticity of Rotorcraft Systems, State College, Pennsylvania, October 1999.

12. Schimke, D., Jänker, P., Blaas, A., Kube, R., Schewe, G., and Keßler, Ch., "Individual Blade Control by Servo-Flap and Blade Root Control: A Collaborative Research and Development Programme," 23rd European Rotorcraft Forum, Dresden, Germany, September 1997.

13. Poling, D.R., "1/5th Scale Model 360 DNW Rotor Blade Structural Properties and Airfoil Tables," Boeing Document 8-1160-0215, June 1992.

14. Straub, F.K. and Johnston, R.A., "Aeroelasticity and Mechanical Stability Report, 0.27 Mach Scale Model of the YAH-64 Advanced Attack Helicopter," NASA CR 178284, May 1987.

15. Drela, M., "Newton Solution of Coupled Viscous/Inviscid Multielement Airfoil Flows," AIAA Paper 90-1470, June 1990.

16. Wong, Raymond and van Dam, C.P., private communication, September 2000.

17. Domzalski Machine, "Deformable Trailing Edges and Smart Material Actuation for Active Control of Rotor Blades," Phase II SBIR, Contract DAAH10-99-C-0022, private communication.

18. Johnson, Wayne, "Technology Drivers in the Development of CAMRAD II," AHS Aeromechanics Specialists' Conference, San Francisco, California, January 1994.

Table 1. Rotor Characteristics.

Description	Variable	Value
No. of Blades	b	4
Rotor Radius	R	6.48 ft = 77.76 in
Airfoil Chord	c	5.670 in
Planform		Rectangular
Solidity	σ=bc/π R	0.0928
Twist, Linear	θ_{pt}	-10°
Airfoil		VR-18 with .04 c –3 deg tab
Feathering & Twist Axes		0.27 c
Blade Elastic Axis		0.20 c
Blade Center of Gravity		0.263 c
Blade Tensile Axis		0.263 c
Lag-Flap Hinge Location	e	3.50 in (4.50% R)
Blade Grip Location	r_g	10.530 in (13.54% R)
Root Cutout Location	r_c	22.2 in (28.55% R)
Kinematic Couplings		0
Lag Damping	Dζ	8.48 ft-lb/(rad/s)
Elevon Chord, Plain	cδ	0.850 in (15% c)
Elevon Motion	δ	±5.0 deg at r_δ=.86R
Density, Air	ρ_o	0.002377 slug/ft
Temperature, Air	τ	59 deg F
Speed of Sound, Air	c_{so}	1,116.45 ft/s
Viscosity, Air	μ_o	3.7372 E-7 slug/ft-s
Weight, Passive Blade		2.96 lb
Nominal Rotor Speed	Ω_o	1,070 RPM (17.83 Hz)
Tipspeed, hover	V_{tip}	726.1 ft/s
Mach Number, hover	M_{tip}	0.6504
Reynolds Number, hover	Re_{tip}	2.182 E6

Table 2. Uniform blade section properties (r = 22.2 to 77.76 in), baseline.

Property	Value
EI_{Flap}, lb-in^2	1.095 E5
EI_{Chord}, lb-in^2	4.55 E6
GJ, lb-in^2	1.010 E5
m, lb/in	0.0368
I_θ, lb-in	0.0684

Table 3. Fraction of maximum elevon deflection (Primary and Secondary), resulting elevon-induced hub loads, and fraction of controlled to uncontrolled hub loads, baseline ($\omega_{\phi 1} = 4.79/\text{rev}$), $\mu = .125$.

r_δ/R	0.62	0.66	0.70	0.74	0.78	0.82	0.86	Total	
$\lvert\delta_p\rvert / \lvert\delta_r\rvert$	1.00	1.00	1.00	1.00	0.28	0.25		4.53	
$\lvert\delta_s\rvert / \lvert\delta_r\rvert$					0.72	0.75		1.47	
								6.00	
Elevon-Induced Hub Load (lb or ft-lb)								Total	Controlled/ Uncontrolled
T from δ_o					40			40	0.77
Q from δ_o						5		5	0.75
H from δ_{1x}				14				14	0.81
Y from δ_{1x}	12				10			22	0.77
M_x from δ_{1x}			13					13	0.79
M_y from δ_{1x}		11				9		20	0.74
								AVG	0.77

Table 4. Fraction of maximum elevon deflection (Primary and Secondary), resulting elevon-induced hub loads, and fraction of controlled to uncontrolled hub loads, baseline ($\omega_{\phi 1} = 4.79$), $\mu = .25$.

r_δ/R	0.62	0.66	0.70	0.74	0.78	0.82	0.86	Total	
$\lvert\delta_p\rvert / \lvert\delta_r\rvert$	1.00	1.00	1.00	1.00	0.16	0.16		4.32	
$\lvert\delta_s\rvert / \lvert\delta_r\rvert$					0.84	0.84		1.68	
								6.00	
Elevon-Induced Hub Load (lb or ft-lb)								Total	Controlled/ Uncontrolled
T from δ_o					23			23	0.52
Q from δ_o						3		3	0.54
H from δ_{1x}				14				14	0.53
Y from δ_{1x}	12				11			23	0.56
M_x from δ_{1x}			13			3		15	0.50
M_y from δ_{1x}		11				6		17	0.52
								AVG	0.53

Table 5. Fraction of maximum elevon deflection (Primary and Secondary), resulting elevon-induced hub loads, and fraction of controlled to uncontrolled hub loads, alternate ($\omega_{\phi 1} = 3.3/\text{rev}$), $\mu = .125$.

r_δ/R	0.62	0.66	0.70	0.74	0.78	0.82	0.86	Total	
$\lvert\delta_p\rvert / \lvert\delta_r\rvert$		0.79	0.54	1.00	1.00	1.00	1.00	5.33	
$\lvert\delta_s\rvert / \lvert\delta_r\rvert$		0.21	0.46					0.67	
								6.00	
Elevon-Induced Hub Load (lb or ft-lb)								Total	Controlled/ Uncontrolled
T from δ_o		65						65	0.61
Q from δ_o			8					8	0.56
H from δ_{1x}							33	33	0.55
Y from δ_{1x}						33		33	0.65
M_x from δ_{1x}		3		21				25	0.61
M_y from δ_{1x}			9		23			32	0.55
								AVG	0.59

Table 6. Fraction of maximum elevon deflection (Primary and Secondary), resulting elevon-induced hub loads, and fraction of controlled to uncontrolled hub loads, alternate ($\omega_{\phi 1} = 3.3/\text{rev}$), $\mu = .25$.

r_δ/R	0.62	0.66	0.70	0.74	0.78	0.82	0.86	Total	
$\lvert\delta_p\rvert / \lvert\delta_r\rvert$		0.44	0.50	0.85	1.00	1.00	0.76	4.55	
$\lvert\delta_s\rvert / \lvert\delta_r\rvert$		0.00	0.00	0.00			0.24	0.24	
								4.79	
Elevon-Induced Hub Load (lb or ft-lb)								Total	Controlled/ Uncontrolled
T from δ_o		36						36	0.00
Q from δ_o			8					8	0.00
H from δ_{1x}							25	25	0.00
Y from δ_{1x}						33	6	39	0.04
M_x from δ_{1x}				18				18	0.00
M_y from δ_{1x}					23			23	0.03
								AVG	0.01

Table 7. Total fraction of all elevon deflections (equivalent number of standard elevons) and resulting fraction of controlled to uncontrolled hub loads, baseline ($\omega_{\phi 1} = 4.79/\text{rev}$).

	μ = .125	μ = .25		
Type of Elevons	Standard	Standard		Big
Equiv. No. of Std. Elevons	6.00	6.00	10.00	10.30
T (Thrust)	0.77	0.52	0.31	0.19
Q (Torque)	0.75	0.54	0.31	0.19
H (Longitudinal Force)	0.81	0.53	0.31	0.18
Y (Lateral Force)	0.77	0.56	0.28	0.19
M_x (Roll Moment)	0.79	0.50	0.26	0.20
M_y (Pitch Moment)	0.74	0.52	0.27	0.20
AVG	0.77	0.53	0.29	0.19

Table 8. Total fraction of all elevon deflections (equivalent number of standard elevons) and resulting fraction of controlled to uncontrolled hub loads, alternate ($\omega_{\phi 1} = 3.3/\text{rev}$).

	μ = .125	μ = .25	
Type of Elevons	Standard	Standard	
Equiv. No. of Std. Elevons	6.00	3.70	4.79
T (Thrust)	0.61	0.20	0.00
Q (Torque)	0.56	0.20	0.00
H (Longitudinal Force)	0.55	0.20	0.00
Y (Lateral Force)	0.65	0.20	0.04
M_x (Roll Moment)	0.61	0.20	0.00
M_y (Pitch Moment)	0.55	0.20	0.03
AVG	0.59	0.20	0.01

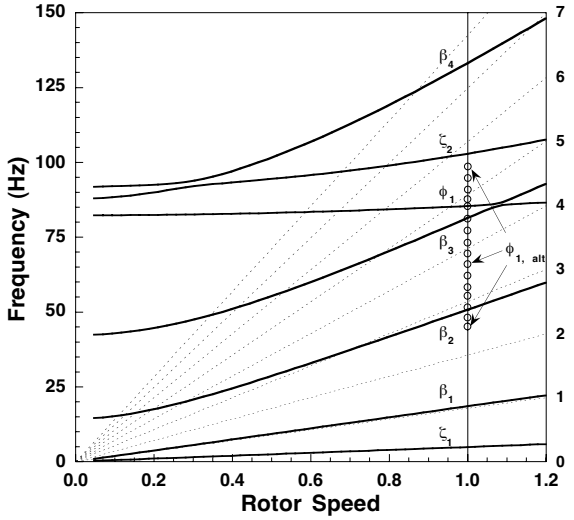

Figure 1. Rotor blade frequencies in a vacuum, 9.5 deg collective pitch, including effect of torsion stiffness on first torsion natural frequency at the nominal rotor speed of 1,070 RPM; β = Flap, ζ = Chord, ϕ = torsion, and subscripts indicate mode number.

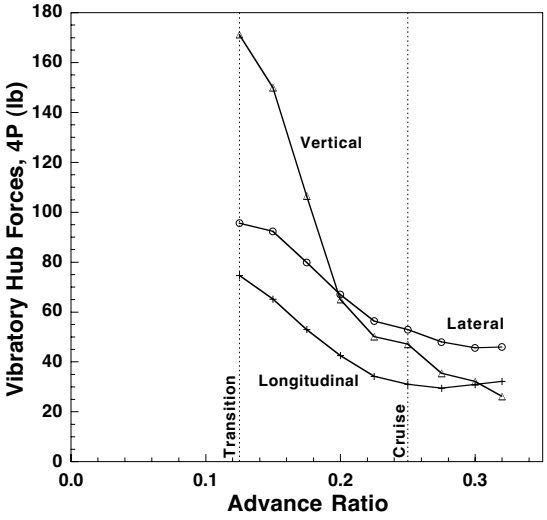

Figure 2. Steady-state 4/rev vibratory hub forces (nonrotating frame).

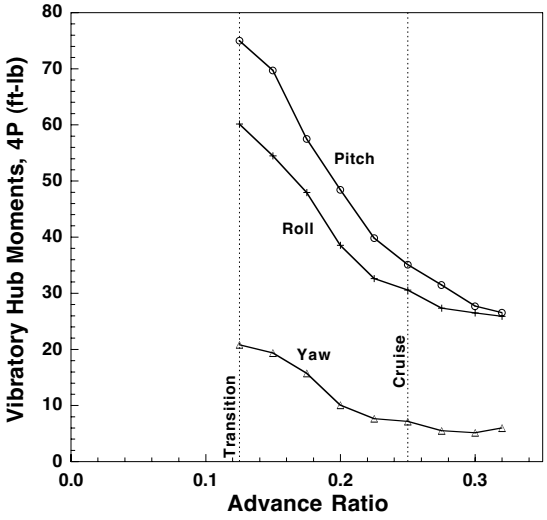

Figure 3. Steady-state 4/rev vibratory hub moments (nonrotating frame).

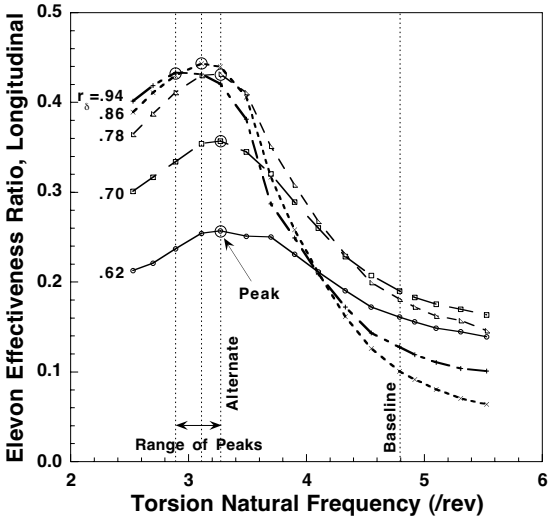

Figure 4. Effect of torsion natural frequency on elevon 4/rev longitudinal force effectiveness for various elevon radial positions, normalized by baseline ($\omega_{\phi 1}$ = 4.79/rev) steady-state 4/rev longitudinal force at $\mu = 0.125$.

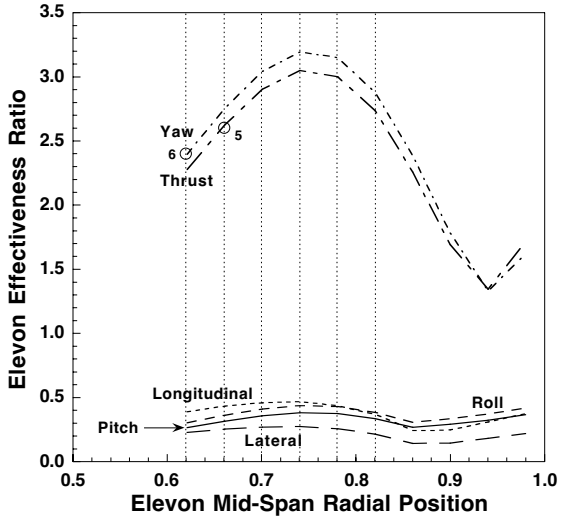

Figure 6. Effect of elevon radial position on elevon effectiveness for reducing 4/rev hub loads for the baseline ($\omega_{\phi 1}$ = 4.79/rev); each hub load is normalized by its corresponding ($\omega_{\phi 1}$ = 4.79/rev) steady-state vibratory load at $\mu = 0.25$.

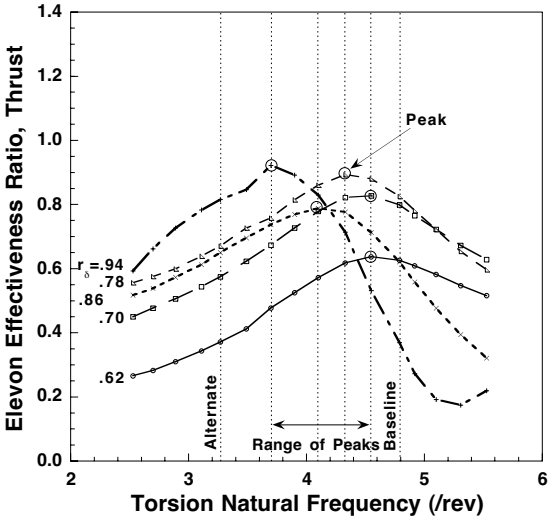

Figure 5. Effect of torsion natural frequency on elevon 4/rev thrust force effectiveness for various elevon radial positions, normalized by baseline ($\omega_{\phi 1}$ = 4.79/rev) steady-state 4/rev thrust at $\mu = 0.125$.

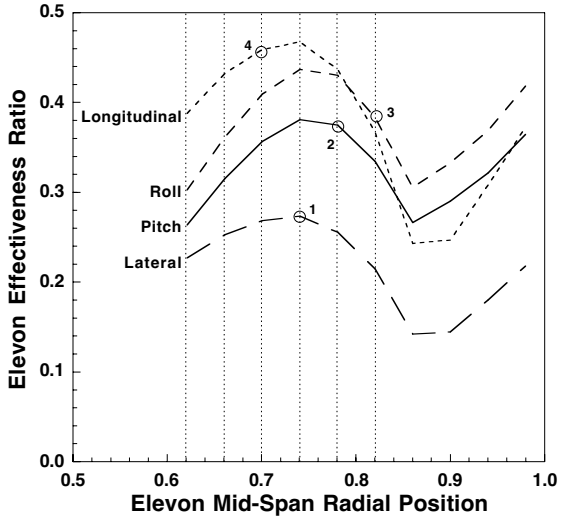

Figure 7. Same data as Figure 6 but with different ordinate scale.

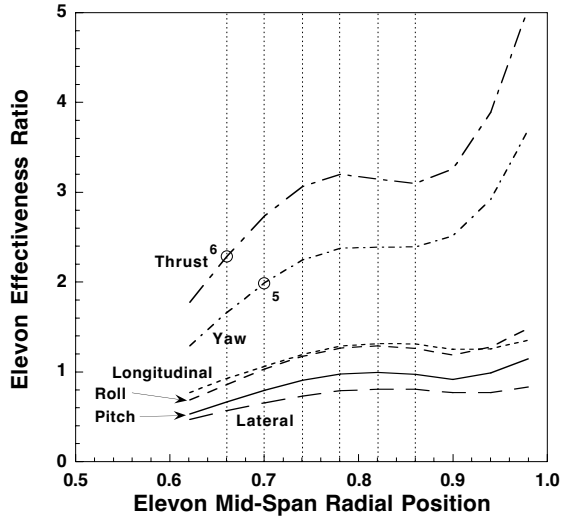

Figure 8. Effect of elevon radial position on elevon effectiveness for reducing 4/rev hub loads for the alternate ($\omega_{\phi 1}$ = 3.3/rev); each hub load is normalized by its corresponding ($\omega_{\phi 1}$ = 3.3/rev) steady-state vibratory load at $\mu = 0.25$.

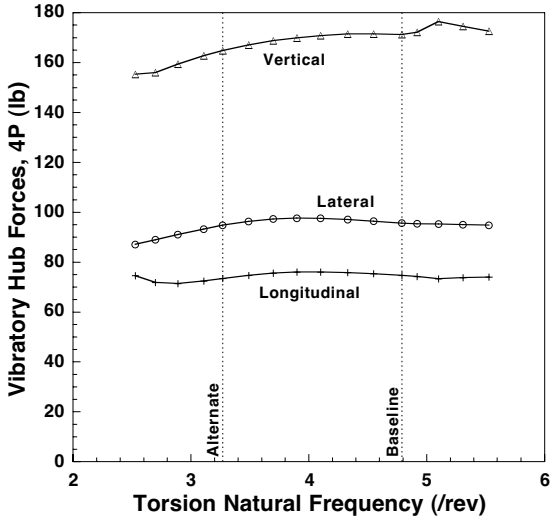

Figure 10. Effect of torsion natural frequency on steady-state 4/rev vibratory hub forces, $\mu = .125$.

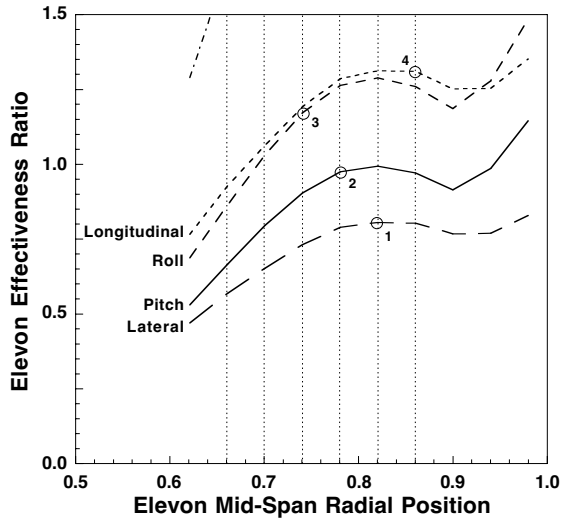

Figure 9. Same data as Figure 8 but with different ordinate scale.

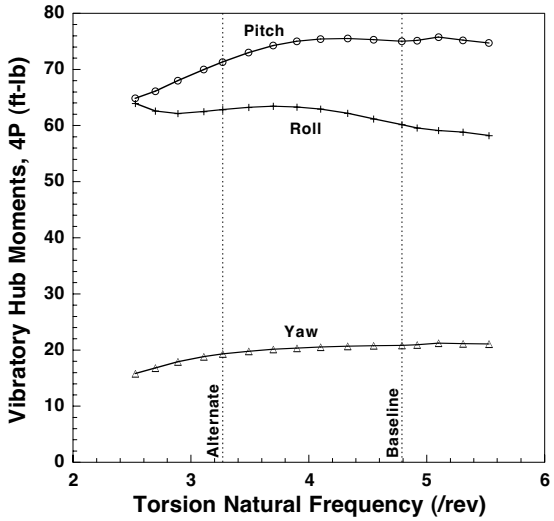

Figure 11. Effect of torsion natural frequency on steady-state 4/rev vibratory hub moments, $\mu = .125$.

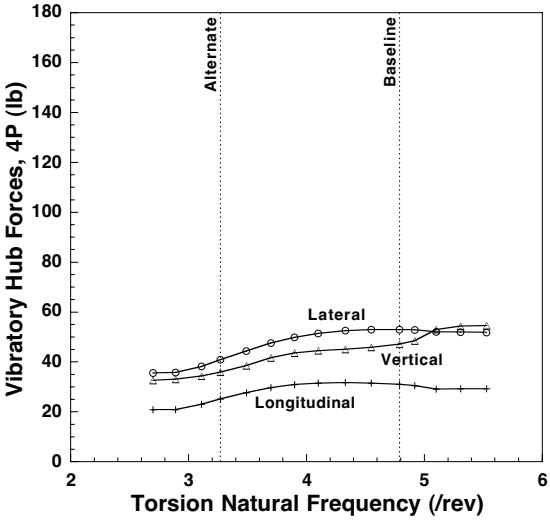

Figure 12. Effect of torsion natural frequency on steady-state 4/rev vibratory hub forces, $\mu = .25$.

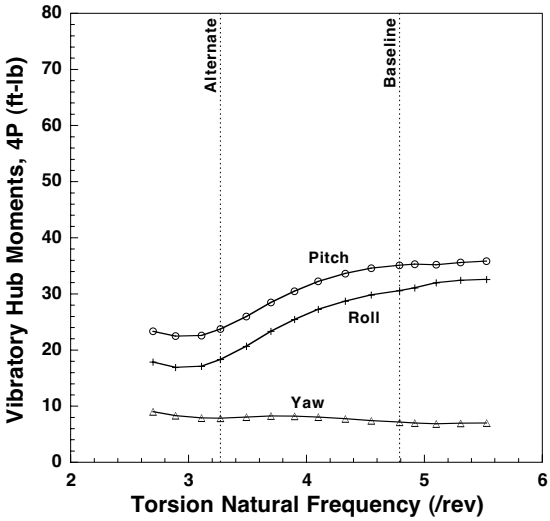

Figure 13. Effect of torsion natural frequency on steady-state 4/rev vibratory hub moments, $\mu = .25$.